Chem Soc Rev

Cite this: *Chem. Soc. Rev.*, 2012, **41**, 6125–6137

www.rsc.org/csr

CRITICAL REVIEW

Benzene-1,3,5-tricarboxamide: a versatile ordering moiety for supramolecular chemistry†

Seda Cantekin,[a] Tom F. A. de Greef[ab] and Anja R. A. Palmans*[a]

Received 23rd April 2012
DOI: 10.1039/c2cs35156k

After their first synthesis in 1915 by Curtius, benzene-1,3,5-tricarboxamides (BTAs) have become increasingly important in a wide range of scientific disciplines. Their simple structure and wide accessibility in combination with a detailed understanding of their supramolecular self-assembly behaviour allow full utilization of this versatile, supramolecular building block in applications ranging from nanotechnology to polymer processing and biomedical applications. While the opportunities in the former cases are connected to the self-assembly of BTAs into one-dimensional, nanometer-sized rod like structures stabilised by threefold H-bonding, their multivalent nature drives applications in the biomedical field. This review summarises the different types of BTAs that appeared in the recent literature and the applications they have been evaluated in. Currently, the first commercial applications of BTAs are emerging. The adaptable nature of this multipurpose building block promises a bright future.

[a] *Laboratory of Macromolecular and Organic Chemistry and Institute for Complex Molecular Systems, Eindhoven University of Technology, PO Box 513, 5600 MB Eindhoven, The Netherlands. E-mail: a.palmans@tue.nl; Fax: +31-40-2453587; Tel: +31-40-2473105*
[b] *Institute for Complex Molecular Systems and Biomodelling and Bioinformatics, Eindhoven University of Technology, PO Box 513, 5600 MB Eindhoven, The Netherlands*
† Part of a themed issue on supramolecular polymers.

1. Introduction

The advent of the field of supramolecular (polymer) chemistry resulted in the design and synthesis of functional molecules that evolve into ordered superstructures with tuneable properties by means of non-covalent interactions between the constituting parts.[1] H-bonding, metal–ion complexation, electrostatic interactions,

Anja R. A. Palmans, Seda Cantekin and Tom F. A. de Greef

Seda Cantekin (middle) received her MSc degree in Chemistry at the Middle East Technical University under the supervision of Prof. Dr M. Balci. Her research focused on the total synthesis of conduritol derivatives which are biologically active. In 2008 she joined the Molecular Science and Technology group and the Institute for Complex Molecular Systems at the Eindhoven University of Technology as a PhD student under the supervision of Prof. Dr E. W. Meijer and dr. ir. A. R. A. Palmans. Her PhD research investigates the limits of supramolecular chirality in synthetic supramolecular polymers and mainly focuses on the combination of chemical reactions with noncovalent interactions.
Tom de Greef (right) obtained an MSc degree in Biomedical Engineering (2004) at the Eindhoven University of Technology (The Netherlands) and continued with a PhD in Chemistry (2009) in the group of Prof. E. W. Meijer and Prof. R. P. Sijbesma at the same university. In 2010 he was appointed assistant professor in the Computational Biology group and the Institute for Complex Molecular Systems at the Eindhoven University of Technology. His research interests range from understanding the fundamental aspects of chemical self-assembly to the forward engineering of complex biochemical systems.
Anja Palmans (left) obtained a degree in chemical engineering (1992) at the Eindhoven University of Technology (The Netherlands) and continued with PhD on the topic of supramolecular chemistry (1997) in the group of Prof. E. W. Meijer. After a Postdoc in the group of Prof. P. Smith at the ETH Zürich (Switzerland) and working at DSM Research (The Netherlands), she became assistant professor in Eindhoven in 2005. Since 2010 she has been an associate professor focussing on the controlled folding of macromolecules with pendant recognition motifs, supramolecular chemistry and the design and synthesis of synthetic enzymes for cascade catalysis.

hydrophobic interactions and combinations thereof are programmed into the molecular structure of the building blocks. Then, under mostly thermodynamically controlled conditions, spontaneous organisation of the building blocks is achieved if suitable conditions are applied. In the last two decades, increasingly complex structures exhibiting a wide diversity of functions have been obtained, highlighting the flexibility and versatility of supramolecular chemistry.

An important prerequisite to evolve from an academic curiosity into a viable platform for advanced, functional materials is the synthetic accessibility of the supramolecular building blocks and an in-depth understanding of how small changes in the molecular structure affect the aggregation properties. In recent years, a large number of supramolecular building blocks have appeared in the scientific literature. Many supramolecular building blocks are only accessible *via* multistep synthesis or show aggregation properties that are either difficult to control or restricted to a small set of conditions. Importantly, a number of motifs emerged such as the ureido-pyrimidinones, peptide amphiphiles and hexabenzocoronenes that allowed exploitation in a variety of applications.[2] Ureido-pyrimidinones, for example, have been commercialised and are currently investigated as materials for regenerative medicine applications.[3] These moieties are used as solid bioactive membranes for the development of a bioartificial kidney and as bioactive hydrogels for drug delivery and tissue engineering applications.[4,5]

This review focuses on the benzene-1,3,5-tricarboxamide (BTA) motif comprising either three N-centred or three C=O centred amides attached to a benzene core (Fig. 1). Such BTAs attracted considerable attention in the last few years in supramolecular chemistry. The three amide bonds are capable of H-bond formation, and – under selected conditions – one-dimensional growth of the monomers into supramolecular polymers is achieved (Fig. 2). After a brief overview of synthetic approaches towards N-centred and C=O centred BTAs, we will discuss the details of the H-bond formation in the bulk and in solution. Studies conducted to unravel the mechanism of the cooperative self-assembly behaviour and the origin of the cooperativity in this system have contributed enormously in understanding the scope and limitations of H-bond based self-assembly processes. Finally, we will address how BTAs have found their way into a variety of applications, notably in the field of advanced, nanostructured materials and as scaffolds in biomedical applications.

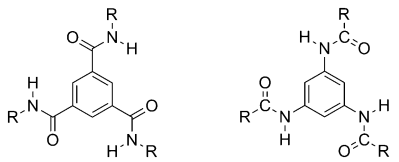

Fig. 1 General chemical structures of C=O- and N-centred benzene-1,3,5-tricarboxamide (BTA) molecules.

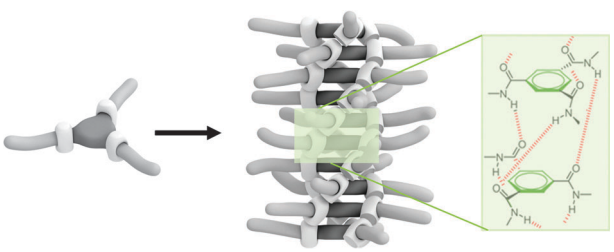

Fig. 2 Schematic representation of benzene-1,3,5-tricarboxamide self-assembly into helical one-dimensional aggregates, which are stabilised by threefold intermolecular H-bonding.

2. Structure and synthesis of benzene-1,3,5-tricarboxamides

2.1 Synthetic approaches to BTAs

Benzene-1,3,5-tricarboxamide molecules consist of a benzene core and three amides connected to the benzene ring at the 1,3 and 5-position. The amide group is attached to the benzene ring *via* the nitrogen, giving rise to N-centred BTAs or *via* the carbonyl group, yielding C=O-centred BTAs (Fig. 1). The R groups in BTAs can be aliphatic or aromatic, polar or apolar, charged or neutral, chiral non-racemic, racemic or achiral. When the functional groups connected to the amides are identical, the BTA molecules are C_3 symmetric. BTAs can also be desymmetrised by introducing different functionalities on the amide groups.

The first BTA molecule was reported in 1915 by Curtius (Scheme 1).[6] Curtius used benzene-1,3,5-tricarboxylic acid as the starting material. The triacyl triazide, which is explosive under light pressure and mild heating, was obtained *via* the triester. The triacyltriazides were then treated with aniline resulting in the formation of a triphenyl substituted BTA. The highly explosive triacyl triazide, however, does not allow large scale preparation of BTAs. Alternatively, Rohm and Haas patented in 1954 the preparation of the tris(vinyloxyethyl) BTA analogue, starting from trimethyl benzene-1,3,5-tricarboxylate and 2-vinyloxyethylamine. This amidation reaction required high reaction temperatures and rather long reaction times.[7] In 1959, the tris(*ortho*-nitrophenyl) analogue was obtained in a two-step synthesis. Trimesic acid was first treated with thionyl chloride, and the acid chloride formed reacted with an amine at room temperature.[8] This synthetic procedure significantly reduced the reaction time, as a result of the reactive acid chloride intermediate. In fact, the most common synthetic strategy to prepare C=O-centred BTAs at the moment is the reaction of benzene-1,3,5-tricarbonyl trichloride (trimesic chloride) with the appropriate amine in the presence of base, although direct functionalisation of benzene-1,3,5-tricarboxylic acid with the appropriate amine by using suitable coupling agents is also frequently applied.

Desymmetrised C=O-centred BTA molecules were reported for the first time in 1975 and patented by Bayer.[9] More recently,

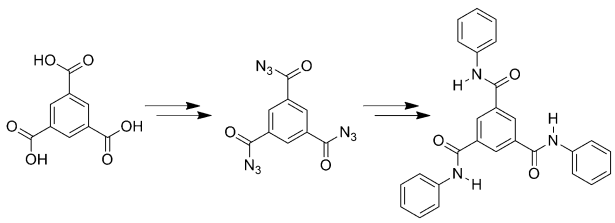

Scheme 1 Synthesis of the first BTA molecule by Curtius.[6]

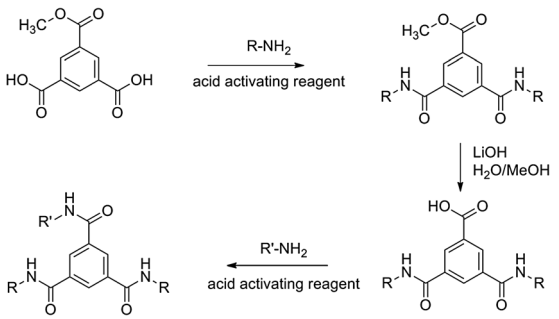

Scheme 2 Synthesis of desymmetrised BTAs.

Meijer and coworkers reported the synthesis of 3,5-(methoxycarbonyl)isophthalic acid *via* dihydrolysis of trimethyl benzene-1,3,5-tricarboxylate.[10] This synthetic strategy allows easy access to alkyl-substituted desymmetrised BTAs in 3 additional steps (Scheme 2).

The first N-centred BTA was synthesized in 1949 *via* the catalytic hydrogenation of 1,3,5-trinitrobenzene with RANEY® nickel in ethyl acetate.[11] A similar technique for the preparation of N-centred BTAs was reported by Steffens *et al.* in 1970 by applying palladium on carbon as the catalyst.[12] However, handling of 1,3,5-trinitrobenzene is tedious and 1,3,5-triaminobenzene is prone to degradation. An alternative synthetic approach was reported in 1981 by Muramatsu and coworkers in order to prevent these synthetic struggles. In the new method, unexplosive and readily available phloroglucinol trioxime was used as the starting material (Scheme 3, top).[13] Consecutive acetylation and reduction of this compound resulted in the desired *N,N′,N″*-(benzene-1,3,5-triyl)triacetamide in good yields. Later, another method was introduced by van Gorp *et al.* starting from commercially available 3,5-dinitroaniline from which desymmetrised end products are readily available (Scheme 3, bottom).[14]

2.2 BTA structures

Over the past decades, a broad range of N- and C=O-centred BTA molecules have been synthesized and analyzed in detail. BTA structures derivatised with R-groups such as alkyl,[15,16] aryl,[17–19] pyridyl,[20] bipyridyl,[21,22] porphyrinyl,[23] triphenylyl,[24] oligo(*p*-phenylenevinylene),[25] amino acid,[26–31] dipeptide,[32] oligopeptide,[33] oligo(ethyleneoxy),[34,35] and benzocrown ethers[36] have been procured. The BTA derivatives have been investigated in a large variety of applications such as organogels,[37] hydrogels,[18,36,38] liquid crystals,[15] nanostructured materials,[39] MRI contrast reagents,[40] nucleating agents for polymers,[41] metal complexation reagents,[29] and microcapsules for drug delivery[42] (Fig. 3). Furthermore, macrocyclic[43–46] and dendritic[47–53] BTA containing topologies have been prepared although they often require lengthy synthetic procedures. Recently, BTAs have been incorporated into polymers. Telechelic polymers, end-capped with BTAs, show thermoplastic elastomeric behaviour, typical for soft rubbery materials.[10] Poly(methacrylate)s with pendant BTA units fold into well defined single chain polymeric nanoparticles and have been used as nanoreactors for efficient catalysis.[54,55]

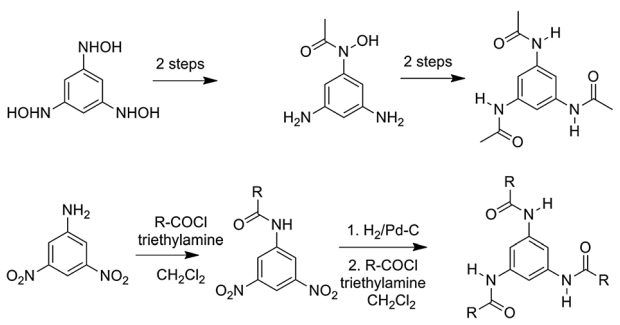

Scheme 3 (top) Synthesis of N-centred BTAs starting from phloroglucinol trioxime. (bottom) Synthesis of N-centred BTAs starting from 3,5-dinitroaniline.

The nature of the side chain is important for the potential application area of the BTA molecules. For example, BTAs comprising bulky, aliphatic side chains are high melting crystalline solids, which crystallise as fibre-like needles. These characteristics make BTAs effective clarifying and nucleating agents for isotactic polypropylene (Fig. 3A).[41,56] In contrast, long alkyl side chains induce thermotropic liquid crystalline behaviour (Fig. 3B)[15,57] and branched alkyl side chains result in organogel behaviour (Fig. 3C).[37] Compatibility with water is achieved by introducing charged Gd(III) complexes at the periphery,[28] ethyleneoxide based side chains[35] or acidic groups.[18,26] The former (Fig. 3D) are currently explored as MRI contrast agents.[40] While BTAs are stable, also under aqueous conditions, the introduction of water-labile groups is easy and allows the preparation of microcapsules that hydrolyse over time and release their cargo into the environment (Fig. 3E).[42] Fluorescent BTAs have been obtained by functionalisation with conjugated moieties.[22,25,58] Interestingly, the introduction of chiral non-racemic, soluble alkyl side chains leads to the formation of a one-dimensional aggregate with a preferred helical sense.[59] This has allowed a detailed characterization of the aggregation properties and the mechanism by which aggregation occurs, by using sensitive spectroscopic techniques such as circular dichroism (see Section 4.1).

3. BTAs in the solid state

3.1 Crystal structure analysis of BTAs

Depending on the nature of the side chains, different types of crystal structures and packing have been obtained for BTAs. An overview of BTA molecules with reported crystal structures is given in Scheme 4. The first two crystal structures of C=O-centred BTAs appeared in 1997. *N,N′,N″*-Trimethyl-1,3,5-benzenetricarboxamide (**1**) crystallises in a monoclinic $P2_1$ crystal lattice in which the three amides are involved in NH···OC intermolecular H-bonding.[60] One H-bond is formed between molecules within one stack while two additional H-bonds are responsible for the lateral interactions between the amides of the molecules within different stacks (Fig. 4a). In contrast, pyridine BTA derivative **2** crystallises in a *P* space group and forms an infinite two-dimensional honeycomb grid consisting of bilayer sheets.[20] H-bonds occur between the amide hydrogen and the pyridine nitrogen leading to the formation of pores with a diameter of approximately 8.2 Å, which are filled with disordered methanol molecules. Interestingly, the packing of compound **2** in the crystals obtained from

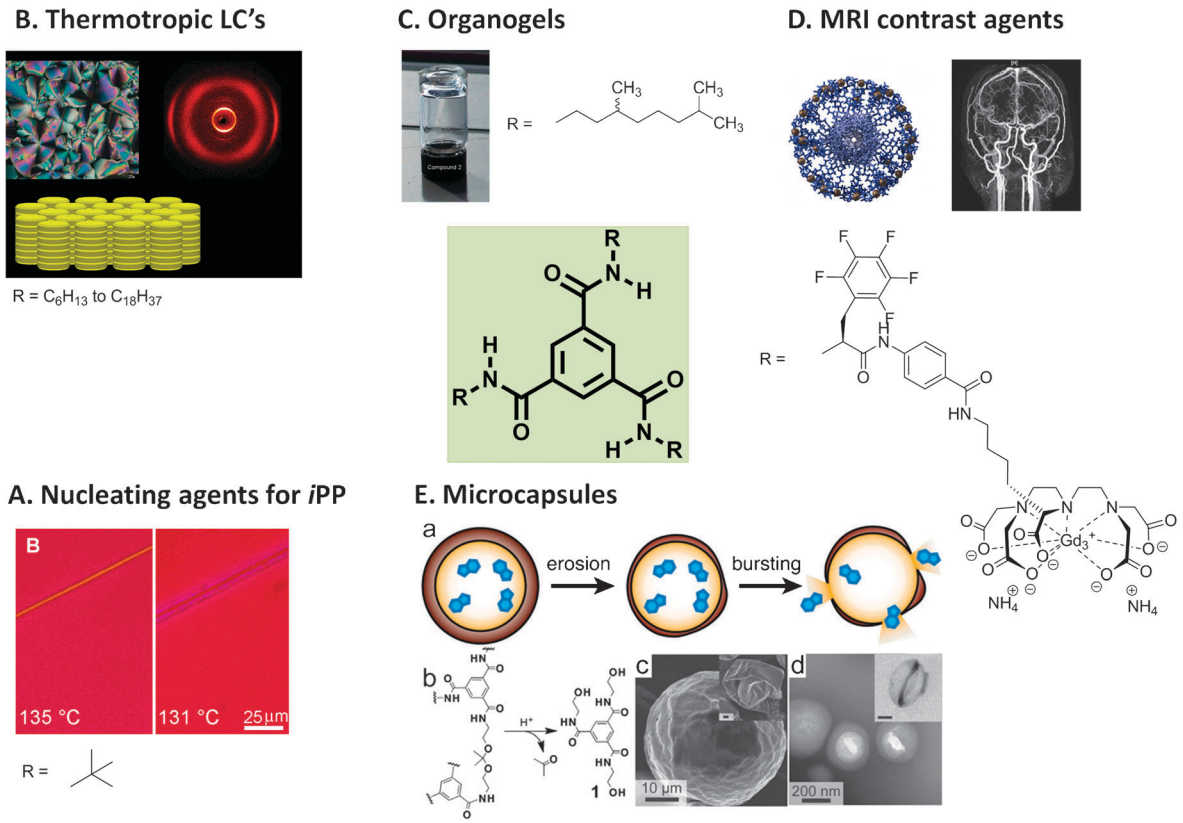

Fig. 3 An overview of the application areas for BTAs. Different side chains attached to the BTAs result in different applications. (A) Reprinted with permission from ref. 41. Copyright (2005) American Chemical Society. (E) Reproduced from ref. 42 with permission from the Royal Society of Chemistry.

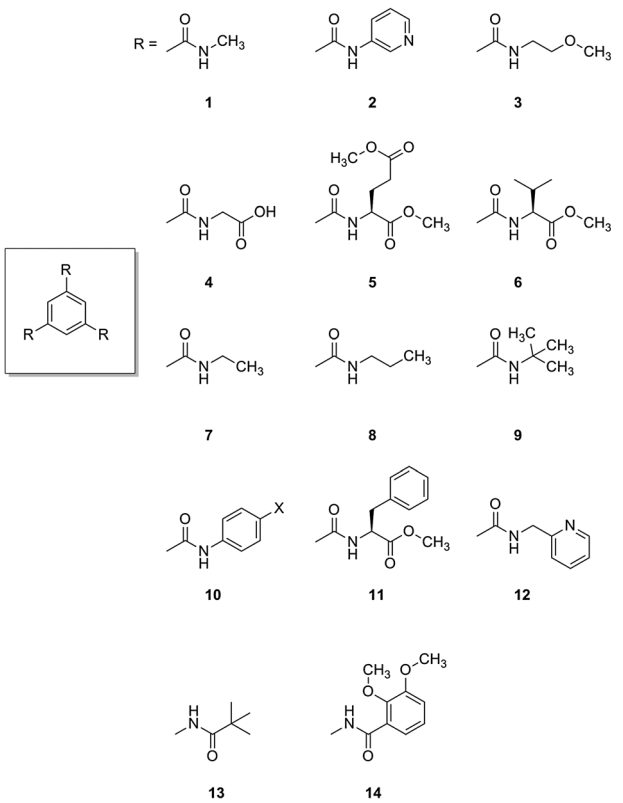

Scheme 4 Selected chemical structures of BTAs with reported crystal structures. For compound **10**: X = F, Cl, Br or I.

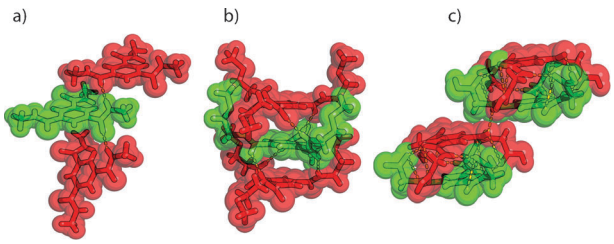

Fig. 4 Crystal structures of (a) *N*,*N*′,*N*″-trimethyl-1,3,5-benzenetricarboxamide **1**; (b) *N*,*N*′,*N*″-tris(2-methoxyethyl)-1,3,5-benzenetricarboxamide **3**; (c) *N*,*N*′,*N*″-tris(carboxymethyl)-1,3,5-benzenetricarboxamide trihydrate **4**.

MeOH is very sensitive to the concentration applied during crystallisation. Apart from the honeycomb-type crystal structure, two other polymorphs containing H_2O were obtained. The crystal structure of one of these showed NH···OC intermolecular H-bonding and a loss of C_3 symmetry.[61] In 1999, the crystal structure of compound **3** was published by Lightfoot *et al.*[62] The crystal structure revealed the formation of helical supramolecular columnar structures in the solid state as a result of threefold H-bonding between the amides of consecutive discs (Fig. 4b). Although aromatic amides prefer coplanarity[63] of the carbonyl with the aryl to optimise conjugation, in **3** the amides are partially tilted—all in the same direction—as a result of the competition between the demand of conjugation (between carbonyl and aryl) and that of intermolecular H-bonding. The three amides make torsion

angles of 36.8°, 42.4°, and 45.5° with the aryl mean plane giving rise to a propeller-shaped BTA. Later, crystal structures of BTAs **4–14** (Scheme 4) were reported.[26,27,56,64–68] The crystal structure of *N*,*N*′,*N*″-tris(carboxymethyl)-1,3,5-benzenetricarboxamide trihydrate (**4**) was studied by Gong *et al*.[26] The triacid molecule **4** crystallizes in a centrosymmetric space group and a three-dimensional H-bonding network is observed. BTA derivative **4** has a low energy conformation in which all three acid groups are pointed to one side of the plane of the benzoid ring. Such a conformation results in a self-complementary shape of the molecule, which facilitates dimerization (Fig. 4c). The dimerization between the two triacid molecules results in the formation of extended sheets through H-bonding interactions with water molecules.

As for the crystal structures of BTAs comprising bulky side chains (*e.g*. **5**, **6**, **9** and **10**), a columnar packing similar to that of **3** was typically observed. Ruiz-Perez and coworkers presented an insightful study on various symmetric C=O-centred BTA derivatives with short methyl (**1**), ethyl (**7**) and propyl (**8**) side chains.[64] The solid-state structures of the corresponding molecules confirm that the H-bonding between the NH and CO plays a dominant role in the supramolecular framework in each case, although there are remarkable differences in crystal packing. While methyl and ethyl substituted BTAs (**1** and **7**) form supramolecular sheets, the substituted derivative (**8**) organizes into a H-bonded primitive cubic three-dimensional network. Schmidt and coworkers found that the *tert*-butyl derivative **9** crystallises as columnar structures stabilised by helical, threefold H-bonding, similarly to compound **3**.[56]

Aromatic units included in the BTA structure tend to induce different types of packing, presumably as a result of additional π–π interactions between the aromatic parts. However, when additional halogens are present as is the case in BTA **10** (X = F, Cl, Br or I), triple helical columns stabilised by N–H···O=C H-bonds are found.[65] In addition, halogen···halogen interactions drive the formation of a honeycomb network with pore sizes of 41.4 Å when X=Cl, Br or I. In the fluoro derivative, the packing of the columns is very compact and the fluorophenyl rings of neighbouring columns are interdigitated.

While N- and C=O-centred BTAs have the same number of amide bonds, the strength and directionality of the H-bonding pattern likely differ. However, only a few crystal structures have been reported for N-centred BTAs so far. Attempts to obtain suitable single crystals for 1,3,5-tris(2,2′-dimethylpropionylamino)benzene **13** (Scheme 4) failed because of its microcrystallinity. Nevertheless, the crystal packing of **13** was elucidated using a combination of powder X-ray diffraction and solid state NMR.[69] The space group $P2_12_12_1$ was assigned. In the crystals, the BTAs are organised in helical columns stabilised by threefold hydrogen bonding. Interestingly, the torsion angle between the amide group and the benzene ring is significantly lower in the case of **13** (around 30°) compared to its CO centred analogue **9** (around 50°), and the intermolecular N–H···O=C distance is around 0.3 Å higher for **13** compared to **9**, indicating a lower H-bond strength in the N-centred BTA. In contrast, the crystal structure for catechol derivative **14** shows a fully coplanar arrangement of the amide with respect to the central benzene core, as a result of the conjugation of the amide with the benzene ring.[70] No columnar intermolecular H-bonds were observed in this structure.

3.2 Infrared spectroscopy

IR spectroscopy is a sensitive tool to investigate the organisation of the intermolecular H-bonding of BTAs in the solid state, and is especially useful when crystal structures are not available. By measuring the IR spectrum of **3**—the crystal structure of which is known—vibrations at 3240 cm^{-1} (N–H stretch), 1640 cm^{-1} (C=O stretch) and 1560 cm^{-1} (amide II stretch) are unambiguously assigned to the threefold H-bonding between neighbouring BTA molecules within the columnar structures.[57] In contrast, compound **1** shows a completely different IR spectrum *i.e*., two sharp N–H stretch vibrations are found at 3333 and 3259 cm^{-1} while the amide II band is observed at 1539 cm^{-1}. The two different types of H-bonds (one between molecules within a column and the other laterally between molecules of different columns) observed in the crystal structure of **1** is clearly reflected in the different IR vibrations for N–H stretch and amide II band.

With the help of the IR data gathered for BTAs **1** and **3**, the nature of intermolecular H-bonding in various C=O-centred BTAs (Scheme 5, **15**, **16** and **19–27**) was investigated in the solid-state and in the liquid crystalline (LC) state.[57] All LC BTA derivatives show Col_{ho} phases and the IR spectra in the LC state are typical for a threefold intermolecular H-bonding pattern. However, in the crystalline state of some of the BTAs, different IR spectra were observed, which implies a different crystal packing. For example, the IR spectrum of **15** showed

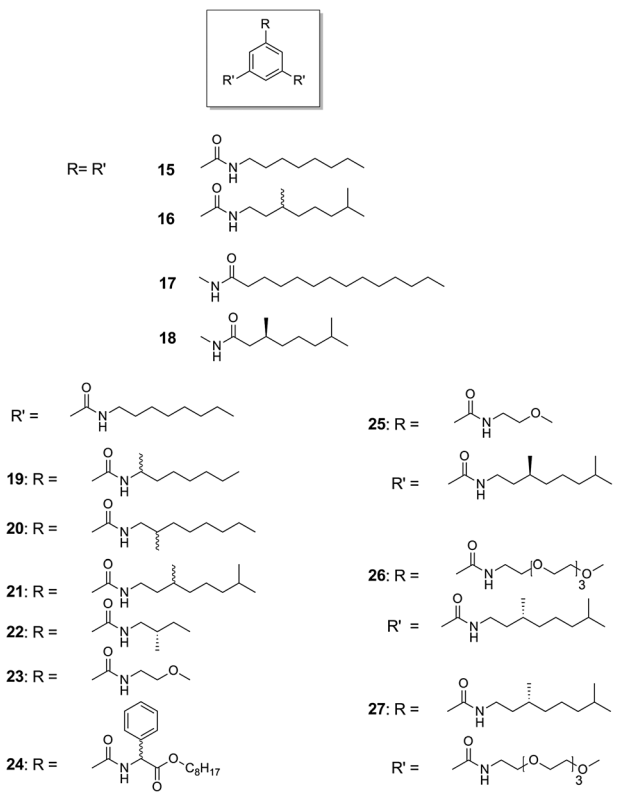

Scheme 5 Chemical structures of various BTAs.

the N–H stretch at 3300 cm^{-1} and the amide band at 1531 cm^{-1} after standing for several days at room temperature suggesting the absence of threefold intermolecular H-bonding. A similar effect was observed in BTAs (*R*)- and (*S*)-**21**. Temperature-dependent IR measurements suggest that for BTAs **15**, (*R*)- and (*S*)-**21** the C_3-symmetrical packing is not thermodynamically stable state at room temperature. While the C_3-symmetrical packing is dominant in the liquid crystalline state, presumably space filling effects dominate the packing in the solid state.

When more polar oligo(ethylene glycol) side chains were introduced into the BTA molecules, the H-bonding pattern changes in the solid state as evidenced by IR spectroscopy.[35] In the presence of a single tetra(ethylene glycol) substituent in the side chains of BTAs (**26**), the threefold intermolecular H-bonding is present, giving rise to an N–H stretch at 3238 cm^{-1} and C=O stretch at 1637 cm^{-1}. However, in the presence of di- (**27**) and tri-tetraethylene glycol units, the N–H stretch appears at 3331 cm^{-1} and 3334 cm^{-1} and C=O stretch at 1655 cm^{-1} and 1656 cm^{-1} suggesting the loss of threefold intermolecular H-bonding. This result indicates a lack of columnar order in these compounds at room temperature, which was attributed to competitive intramolecular H-bonding between ethylene glycol oxygen and amide hydrogen of the tricarboxamide core.

The solid state IR spectra of phenylalanine substituted symmetric BTAs[31] (**11**) and phenylglycine substituted desymmetrised BTAs[71] (**24**) gave rise to typical NH, amide I and amide II vibrations (at 3231, 1638 and 1558 cm^{-1} for **11** and at 3240, 1640, 1550 cm^{-1} for **24**) confirming the presence of threefold intermolecular H-bonding. These results imply that the presence of bulky benzyl or phenyl groups next to the amide core does not necessarily affect the H-bonding pattern in BTAs. Importantly, the gel state of **26** in decahydronaphthalene (5 wt%) led to comparable IR spectra (NH stretch at 3220, amide I at 1634 and amide II at 1558 cm^{-1}) to that of the solid state.[72] This indicates that threefold H-bonding is preserved in the gel state.

IR studies on N-centred BTAs **17** and **18** revealed a different solid-state behaviour compared to that of C=O-centred BTAs: all N-centred BTAs with linear alkyl side chains (for example compound **17**, Scheme 5) were obtained as crystalline solids, only branched derivatives (compound **18**, Scheme 5) showed liquid crystalline behaviour and a Col_{ho} phase was assigned between 91 and 224 °C.[16] The IR spectrum of crystalline **17** at room temperature shows a NH stretch at 3278 cm^{-1} while the C=O vibration is observed as two peaks at 1649 and 1607 cm^{-1} and amide II appears at 1551 cm^{-1}. This result suggests that the typical intermolecular threefold H-bonding pattern is absent in crystalline **17**. Temperature-dependent IR spectroscopy on compound **18** revealed that in the LC state the NH vibration occurs at 3250 cm^{-1} while the C=O vibration and amide II are present at 1651and 1523, respectively. The latter was assigned to the presence of threefold H-bonding in the liquid crystalline state of **18**. The columnar arrangement of the molecules is retained after cooling to room temperature; however, in the crystalline state it slowly rearranges back to a packing in which the threefold H-bonding was absent.

3.3 Solid state NMR

Solid-state NMR spectroscopy can provide valuable information about the supramolecular organization of BTA derivatives when X-ray diffraction of high quality crystals cannot be performed. Spiess and coworkers investigated the solid-state organization and dynamics of C=O-centred BTAs **3**, (*S*)-**16** and N-centred BTA (*S*)-**18** using solid state NMR in combination with Car–Parrinello Molecular Dynamics (CPMD) simulations.[73] Comparison of the ^{1}H-MAS and $^{13}C^1H$ REPT-HSQC spectra of C=O-centred BTAs **3** and (*S*)-**16** shows strong similarities indicating that the branched, chiral side chain of BTA (*S*)-**16** does not result in a different crystal packing compared to the helical columnar packing motif observed in the crystal structure of C=O-centred BTA **3**. Further evidence for this helical, C_3 symmetrical packing motif held together by threefold H-bonding was obtained by a comparison of the chemical shifts in solution ($CHCl_3$) and in the solid state. Compared to the chemical shifts in solution, the ^{1}H-MAS shows a large upfield shift (>1 ppm) for the aryl protons and a large downfield shift (>2 ppm) of the N–H protons suggesting strong H-bonding and π–π interactions in the solid state. Furthermore, *ab initio* NMR chemical shift calculations show an excellent correspondence of the observed ^{1}H-MAS chemical shifts of C=O-centred BTAs **3** and (*S*)-**16** and a molecular model in which the BTA monomers are arranged in a C_3-symmetrical, helical arrangement in which all three amide groups are oriented in the same direction along the aggregate. Surprisingly, the ^{1}H-MAS spectrum of N-centred BTA (*S*)-**18** shows next to the H-bonded N–H signal, three distinct signals for the aryl protons indicating an asymmetric arrangement of the BTA core in the solid state. Extensive CPDM simulations convincingly show that this is the result of an asymmetric arrangement of the three carbonyl groups resulting in a H-bonded spiral of inverted amide groups winding in an opposite direction along the columnar axis.[73] Schmidt and coworkers recently applied solid state NMR measurements on ^{15}N and ^{13}C enriched BTA derivative **13**, and this in combination with computer simulations and powder X-ray diffraction helped elucidate its crystal structure.[69] The three main interactions in solid state NMR are the chemical shift, the dipolar interaction, and the quadrupolar splitting. The chemical shift and the quadrupolar splitting were used to determine the correct space group, the asymmetric unit, the local symmetry of molecular units in the crystal structure, and dynamical disorder of individual building units. Using adequate pulse sequences, distances between homo- and heteronuclear nuclei and torsion angles were extracted from the dipolar coupling. Compound **13** showed a columnar packing where the pseudo-C_3 symmetric molecules are twisted by 60° due to the 2_1 screw axis. The columns are stabilized *via* moderately strong hydrogen bonds with NH···O distances of roughly 2.0 Å and *via* π-interactions due to a sandwich stacking of the aromatic cores with distances of about 3.4 Å. In contrast to compound (*S*)-**18**, in which one of the three carbonyl groups points in the opposite direction of the two others in the solid state, all carbonyl oxygen atoms point in the same direction in compound **13**, highlighting the importance of the alkyl group in the solid state packing of N-BTAs.

4. Self-assembly of BTAs in dilute solution

4.1 Intermolecular self-assembly

Because of their facile synthesis, a wide range of BTA homologues are accessible which has resulted in systematic and detailed studies on their intermolecular self-assembly in dilute solutions. As a result, the BTA motif has evolved into an ideal model system to understand the effect of structural mutations and the role of solvent on the self-assembly mechanism of supramolecular polymers.[74] Such studies are of great importance for the rational design of molecules that self-assemble into nano-objects of defined structure, stability and shape by the molecular information stored in their chemical structures.

The self-assembly of the parent compound, C=O-centred BTA equipped with achiral and chiral aliphatic side chains, has been studied using a wide variety of different spectroscopic techniques in dilute apolar solvents such as methylcyclohexane (MCH) and linear alkanes. Based on the reported crystal structure,[61] it is expected that C=O-centred BTAs self-assemble in solution by means of strong, threefold H-bonding into helical, one-dimensional aggregates. Circular dichroism (CD) spectroscopy in dilute apolar solutions indeed shows a strong Cotton effect centred around 220 nm when a chiral centre is introduced into the alkyl side chains,[59] confirming the helical nature of BTA aggregates. Further analysis reveals that the chiral methyl group in the aliphatic side chains results in a preference for one helical conformation over the other.[75,76] However, when deuterium/hydrogen substitution was used as the source of chiral information, only a small energy difference between the diastereomerically related right- and left-handed helical aggregates was observed.[76] A detailed study on dilute solutions of chiral BTA, (*R*)-**16** (Scheme 5), employing a combination of vibrational circular dichroism (VCD) and CD, supported by DFT calculations confirms the correspondence between the reported[62] crystal structure and the structure of the helical aggregates formed in dilute, apolar solutions.[75] Importantly, the excellent correspondence between the VCD experiments in solution and density functional theory (DFT) calculations clearly provides evidence for a nonzero twist angle between the amide plane and the benzene plane for BTA monomers present in the helical aggregate. As intermolecular H-bonding is the dominant non-covalent interaction responsible for BTA self-assembly, addition of competing solvents such as acetonitrile results in complete disassembly of the helical aggregates.[77] Interestingly, side chains that can compete with the threefold H-bonding of the BTA core *via* intramolecular back-folding such as the ethylene glycol side chains in BTA **25** (Scheme 5) also result in a diminished degree of aggregation as evidenced by UV-Vis and CD studies.[35,74]

To rationalize the intermolecular self-assembly mechanism of BTAs, temperature-dependent UV-Vis and CD spectroscopy were performed for dilute solutions of C=O-centred BTAs **15** and (*R*)-**16** (Scheme 5) in heptane.[75] At high temperatures (> 360 K), no Cotton effect is observed suggesting that BTAs are molecularly dissolved in solution and hence not aggregated at these temperatures. CD spectroscopy upon cooling shows the evolution of a Cotton effect reflecting the formation of helical aggregates, while UV-Vis spectroscopy shows a concomitant hypsochromic shift of the absorption

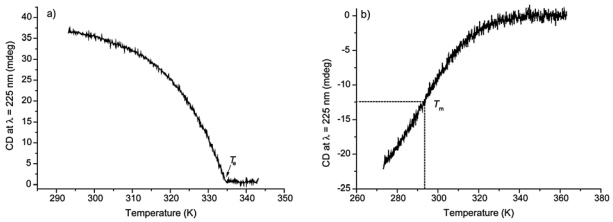

Fig. 5 Melting curves obtained by monitoring the temperature-dependent CD effect at λ = 223 nm: (a) intermolecular self-assembly of BTA (*R*)-**16** in MCH (C_{BTA} = 30 μM) and (b) intramolecular folding of PEGMA/BTAMA (80/20) copolymer **37** in H_2O/2-propanol (C_{BTA} = 50 μM). The melting curves are adapted from ref. 75 and 55, respectively. (a) Reprinted with permission from ref. 75. Copyright (2008) American Chemical Society. (b) Reprinted with permission from ref. 55. Copyright (2011) American Chemical Society.

maximum indicating the formation of H-type aggregates. Detailed information on the self-assembly mechanism was obtained by monitoring the UV-Vis absorption at a single wavelength as a function of temperature for several different total concentrations. The normalized UV-Vis cooling curves exhibit a strong non-sigmoidal shape and a clear elongation temperature (T_e) for all concentrations reflecting the cooperative nature of the self-assembly process (Fig. 5a).[73,75] Analysis[75,78] of the UV-Vis cooling curves was performed using mathematical models for supramolecular polymerizations. The models assume that the aggregation process can be divided into a nucleation regime, described by the equilibrium constant K_2 for dimerization, and an elongation regime, described by the equilibrium constant K ($K_2 \neq K_3 = K_4 \ldots = K_i = K$). Non-linear least square analysis of the experimental melting curves reveals that the cooperative growth is caused by a less favourable enthalpy release during dimerization compared to subsequent monomer addition steps. To uncover the molecular origin of this cooperative effect, quantum chemical calculations in the gas phase were performed on oligomers containing BTA **1** of increasing length.[79,80] These calculations show that cooperativity arises from a combination of long range, non-nearest neighbour dipole–dipole interactions and non-pairwise, short range polarization effects as a result of H-bonding.[79] The dipole–dipole interaction between individual BTA molecules in the helical aggregate is the result of a parallel orientation of the three amide groups along the columnar structure, resulting in a large macro-dipole along the supramolecular polymer.[81]

The detailed understanding of the self-assembly mechanism of helical BTA aggregates in dilute apolar solutions resulted in a number of studies aiming at establishing a correlation between molecular structure, solvent effects and growth of BTA-based helical aggregates. For example, one study specifically addresses the effect of the position of the chiral methyl group in the aliphatic side chains on the cooperative growth of BTA-based helical aggregates.[57] The temperature-dependent CD curves in MCH clearly show a higher T_e, reflecting the increased stability of the helical aggregates, when the methyl group is positioned closer to the core as in BTA **19** (Scheme 5). Importantly, this analysis also shows that the cooperativity of the self-assembly process is not affected by the position of the methyl group in the aliphatic side chains.

Recently, another important single-point mutation in the BTA design was investigated.[16] Employing a combination of CD and UV-Vis spectroscopy, the self-assembly of N-centred BTA (*S*)-**18** (Scheme 5) was investigated in dilute MCH solutions. IR spectra of solid samples showed evidence for the presence of threefold H-bonding in the liquid crystalline state. Similarly, CD spectroscopy in dilute solutions resulted in a strong Cotton effect indicating the formation of helical aggregates. Quantitative analysis of the melting curves acquired by CD spectroscopy using the nucleation–elongation growth model revealed that the enthalpy release in the elongation phase of (*S*)-**18** in MCH is smaller compared to C=O-centred BTAs. In order to rationalize the observed differences in the self-assembly behaviour between C=O- and N-centred BTAs, plane-wave DFT calculations were performed. The DFT calculations revealed that the cohesive energy between two N-centred BTA units in a helical aggregate is lower than the cohesive energy between two C=O-centred BTA units in a helical aggregate which is in agreement with the experimental findings. The difference was attributed to longer and hence less strong H-bonds ultimately caused by a higher energy penalty of rotating the amide group from the plane of the benzene ring upon formation of N-centred BTA helical aggregates compared to C=O-centred BTAs.

The large sensitivity of the CD signal to the conformation of BTA molecules present in the helical aggregate was recently exploited to understand the role of the solvent in the self-assembly process.[82] For this purpose, several C=O-centered BTA monomers were synthesized and studied in the dilute regime using CD and IR spectroscopy in combination with time-dependent DFT calculations in the gas phase. The analysis clearly shows that the solvent plays a critical role in the self-assembly process as evidenced by two different types of Cotton effects observed in linear (*n*-heptane) and cyclic (MCH) alkane solvents, respectively. The two different Cotton effects were related to two distinct BTA conformations within the helical aggregate which differ in their Ph–CO dihedral angle. While the dihedral angle was large in linear alkanes ($\sim 45^\circ$) it was significantly smaller in bulky, cyclic solvents such as MCH ($\sim 35^\circ$). These results were attributed to the intercalation of linear alkanes between the BTA molecules within an aggregate and show the important role of solvent in the growth and stability of self-assembled structures which is a topic of great interest.[83]

In the last decade, several research groups have synthesized BTA analogues and studied their self-assembly under dilute conditions. Nuckolls and coworkers synthesized a large library of hexasubstituted aromatic compounds (*e.g.* **28** and **29** Scheme 6) based on the C=O-centred BTA core.[84–86] It was suggested that the steric congestion of the central core results in a larger dihedral angle between the amide plane and the benzene plane which favours intermolecular self-assembly by H-bonding. CD spectroscopy of compound **28** in dilute dichloromethane–hexane solution showed a strong Cotton effect indicating the formation of helical aggregates.[84] An in-depth solution study was reported on the self-assembly of BTA derivative **29** in various solvents using fluorescence spectroscopy. Surprisingly, the largest helical aggregates are obtained in dichloromethane whereas almost no aggregation

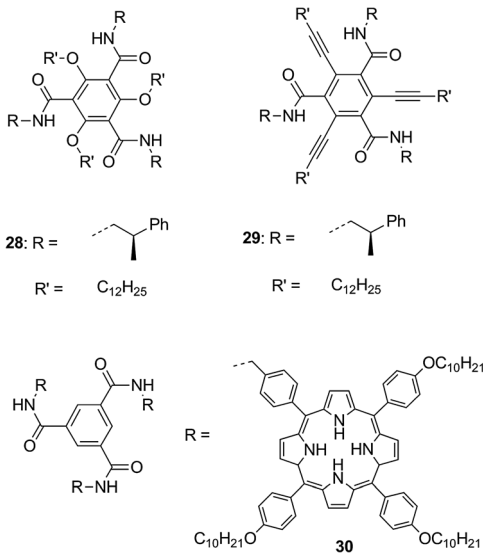

Scheme 6 Chemical structures of BTAs with increased π–π surface.

was observed in dodecane, in sharp contrast with the self-assembly behaviour of alkyl-substituted BTAs. This important result was explained by the fact that the increased aromatic surface of BTA derivative **29** results in stronger π–π interactions and solvophobic effects leading to stabilisation of the monomers in dodecane *via* solvophobic effects and hence reducing the aggregate length.[86] The self-assembly of BTA derivatives in which the three amides of the BTA core groups are covalently linked to porphyrins substituted with chiral aliphatic side chains (**30**, Scheme 6) has been studied by Nolte and coworkers to understand the self-assembly behaviour at the solid–liquid interface.[87,88] A combination of UV-Vis, CD and dynamic light scattering (DLS) experiments on solutions of chiral BTA derivative **30**, equipped with an (*S*)-chiral aliphatic tail, was performed.[88] DLS analysis provided evidence for the formation of long aggregates in solution. In contrast to the simple CD spectrum of BTA (*S*)-**16** in heptane solution, the CD spectrum of aggregates of BTA **30** in *n*-hexane solutions shows a mixture of several Cotton effects. Importantly, one of the Cotton effects is related to the amide functionality indicating chirality transfer from the periphery of the molecule to the BTA core. Analysis of the other Cottons effects shows that at room temperature the three porphyrins orient in a face-to-face arrangement within the helical aggregate. Again, a distinct difference in the shape of the CD spectra in *n*-hexane and cyclohexane was noted which is presumably due to the intercalation of linear alkanes between the side chains of BTA molecules within the helical aggregate.

While most helical aggregates containing the BTA motif self-assemble by intermolecular H-bonding, several examples have emerged in which the amide H-bonding does not play a dominant role in the intermolecular aggregation process. Meijer and co-workers extensively studied[17,22,89–91] the self-assembly of BTA derivatives in which the amide functionality of the BTA core is covalently coupled to a 3,3′-diamino-2,2′-bipyridine (**31** and **32**, Scheme 7) moiety resulting in strong intramolecular H-bonding as evidenced by high level MP2 calculations on model compounds.[91] As a result, the BTA core adopts a coplanar geometry in which

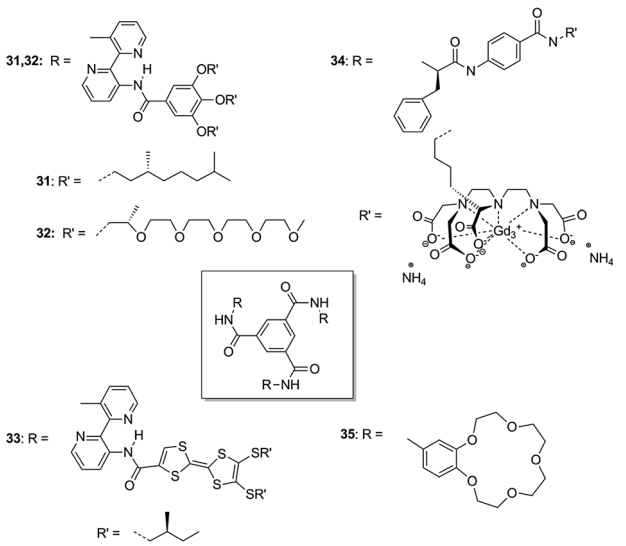

Scheme 7 Chemical structures of BTAs having intramolecular hydrogen bonds (**31–33**) or water-soluble groups at the periphery (**32**, **34**, **35**).

the dihedral angle between the amide plane and the benzene plane is almost zero degree. Due to the large conjugated surface, intermolecular self-assembly in solution takes place *via* strong π–π interactions and solvophobic effects. Strikingly, the melting curves obtained from the temperature-dependent CD spectra of BTA derivative **31** in MCH have a clear sigmoidal shape indicating an isodesmic growth mechanism *i.e.*, the equilibrium constant for monomer addition is independent of the aggregate length.[74,91] This result is attributed to the long-range dipole–dipole interactions induced by rotation of the amide group which are not present in helical aggregates of BTA derivative **31**. Recently, Avarvari and coworkers synthesized and studied the self-assembly of BTA derivative **33** (Scheme 7) in which a tetrathiafulvalene (TTF) moiety, substituted with chiral side chains, is covalently connected to the bipyridine unit.[92] In contrast to apolar bipyridine discotic **31**, BTA derivative **33** shows an intense CD effect in the polar solvent dioxane indicative of a self-assembly process into helical aggregates. Variable temperature CD spectroscopy reveals that at elevated temperatures the aggregates are broken down while detailed analysis of the CD spectrum in combination with extensive molecular modelling shows that the TTF units adopt a twisted conformation with respect to the BTA core in the aggregated state. Due to the slow kinetics, a detailed analysis of the growth mechanism of the self-assembled structures in solution was not possible; however, experimental and theoretical findings reveal that further hierarchical assembly of helical aggregates into coiled superhelices occurs *via* a secondary nucleation mechanism.

In view of the large number of applications, the design and synthesis of self-assembled structures in water is a central goal of supramolecular chemistry.[93–95] In order to design BTA derivatives that self-assemble in water two principal design strategies were explored.[28,96,97] Replacement of the aliphatic side chains of BTA derivative **31** with chiral oligo(ethylene oxide) side chains results in C_3 symmetrical bipyridine discotic **32** which was shown to self-assemble in water into helical structures.[96] The self-assembly of **32** is most probably due to a combination of strong hydrophobic and directional π–π interactions, however, the precise self-assembly mechanism of these structures in water is under investigation. More recently, another design principle was explored based on the principle of hydrophobic shielding.[28,97] In BTA derivative **34**, the L-phenylalanine and aminobenzoate spacer results in a hydrophobic pocket which enables self-assembly of the BTA core *via* triple H-bonding in water as evidenced by NMR spectroscopy. Aqueous solubility is imparted by the highly charged peripheral metal chelate complexes which furthermore provide an additional handle to control the growth of these nanostructures in water.

Detailed spectroscopic studies performed on various analogues of BTA **34** (Scheme 7) reveal that both cooperative, isodesmic as well as anti-cooperative self-assembly may take place depending on the total charge of the metal chelate complexes and the salt concentration.[28,97] This example highlights the rich molecular toolbox available to supramolecular chemists in order to engineer the size, stability and dynamics of self-assembled structures in water. Recently, Kim and coworkers synthesized and studied the self-assembly of benzo-crown ether-substituted BTA **35** (Scheme 7) which was shown to aggregate in DMSO/water.[36] Interestingly, solutions of **35** in DMSO/water exhibit a clear LCST behaviour in the aggregated state at elevated temperatures while the aggregates were shown to be fluorescent.

Since the mechanism of the BTA self-assembly is well understood, these building blocks also serve as an excellent model system to understand the basic principles behind multi-component self-assembly. For example, an equilibrium model capturing the cooperative supramolecular copolymerization of two enantiomerically related BTA monomers was recently developed and excellent correspondence between the theory and experimental findings was demonstrated.[78] Recently, it was also shown that addition of a C_3 symmetric *N*-methylated BTA, that lacks H-bond donating capabilities, to a solution of achiral BTA molecules comprising hexadecyl side chains results in reduced degree of polymerization (DP).[98] Mathematical modelling of the observed process showed that the reduction in DP results from binding of the *N*-methylated BTA to free BTA monomers and end-capping of BTA-based helical aggregates.

4.2 Intramolecular self-assembly

The self-assembly properties of the BTA motif can also be exploited to influence the conformation of macromolecules *via* intramolecular H-bonding. Nuckolls and coworkers designed and studied a series of oligomers based on 2,4,6-trisubstituted C═O-centred BTAs connected to each other *via* various linkers (**36**, Scheme 8).[99] A combined computational and NMR study revealed that a preorganized naphthalene linker (BTA oligomer **36**) resulted in a well-defined folded conformation in which the BTA units are intramolecularly associated *via* threefold H-bonding in dichloromethane. Moreover, it was shown that flexible tethers resulted in less-defined secondary structures. Gong and coworkers synthesized and studied a series of oligomers composed of asymmetric BTAs substituted with chiral side chains and tethered *via* oligoamine linkers.[100]

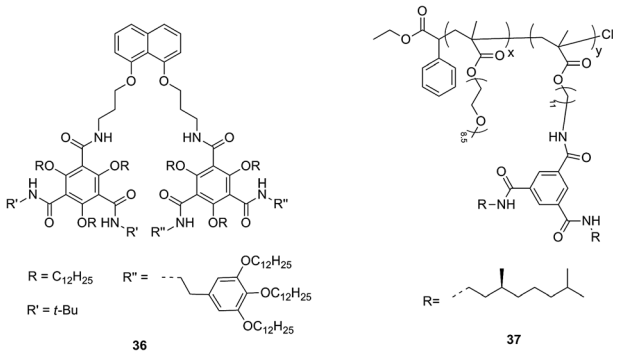

Scheme 8 Oligomeric/polymeric BTA structures.

An experimental study using NMR, vapor pressure osmometry (VPO) and CD spectroscopy combined with DFT calculations convincingly showed that these oligomers are able to adopt folded secondary structures in chloroform, a solvent in which the BTA monomers do not self-assemble *via* intermolecular threefold H-bonding. The folding of a single polymeric chain by copolymerization of chiral BTA-bearing methacrylate (BTAMA) and poly(ethylene glycol) methyl ether methacrylate (PEGMA) was recently demonstrated.[55] Using a wide range of different techniques such as cryo-TEM, CD spectroscopy, dynamic light scattering and diffusion-ordered NMR it was shown that PEGMA/BTAMA copolymer **37** adopts a compact, globular shape in water. The CD spectrum of **37** in water/2-propanol exhibits a bisignate Cotton effect which is similar to those observed in apolar solvents indicating that the BTA monomers are arranged in a helical fashion inside the polymer matrix. CD spectroscopy revealed that, in contrast to the *inter*molecular self-assembly of conventional BTA monomers (**15–23**, Scheme 5) in alkane solvents, the absolute anisotropy value *g* (a concentration-independent measure for the CD-effect) of **37** is independent of the total concentration of BTA units suggesting that self-assembly occurs *within* a single polymeric chain. Furthermore, the temperature-dependent CD spectra of BTAs (**15–23**) in alkane solvents are non-sigmoidal due to cooperative *inter*molecular self-assembly while the corresponding CD curves of **37** in water/2-propanol are sigmoidal (Fig. 5b), a feature commonly encountered in the thermal denaturation of proteins and peptides.

5. Applications of BTAs

5.1 BTAs in material applications

The physical properties of BTAs substituted with aliphatic side chains are strongly influenced by the nature of the side chains. In 1980's, Matsunaga and coworkers showed that BTAs comprising linear alkyl side chains (*n*-hexyl and higher homologues) display thermotropic liquid crystalline behaviour over a broad temperature range and a columnar hexagonally ordered mesophase was assigned.[101] The liquid crystallinity in BTAs has triggered a number of applications in advanced materials. Ferroelectric switching was observed in alkyl substituted BTAs and thin films with remnant polarization and a high surface potential were obtained.[102,103] These materials are of great interest for diodes and nonvolatile memory devices. Remnant polarization and high surface potential are also important for electret materials, which are dielectric materials that exhibit quasi permanent electric fields as a result of trapping of electric charges or by macroscopically oriented dipoles. Binary mixtures of BTAs and polymers showed improved electret properties and constitute an easy and accessible way to produce such materials.[104] In addition, liquid crystalline BTAs equipped with azobenzene chromophores featured a remarkably stable light-induced orientation in thin-film architectures, and are attractive candidates for the fabrication of stable holographic volume gratings.[105] BTAs with peripheral, polymerisable acrylate groups were investigated to prepare surface relief structures *via* photoembossing.[106] The polymerisable BTAs facilitated the process and allowed improvement of the structure height and preparation of relief structures in the micrometer range. Finally, the combination of acid-modified BTAs with polypropylene imine dendrimers resulted in liquid crystalline materials that display a well-ordered superlattice. Materials with well-ordered structures on nanometer length scales are important for a number of applications including nanoporous membranes that show selective transport properties.[39]

Depending on the polarity of the side chains of the BTAs, organogels and hydrogels can be prepared. Hanabusa and coworkers observed that branched side chains derived from (*racemic*)-citronellol induced visco-elastic behaviour upon mixing the BTAs with alkane solvents such as decane.[37,60] Such organogels are interesting candidates to prepare insulating layers for electrical cables.[107] Alternatively, BTAs have been functionalised with peripheral crown ethers (**34**),[36] pyridines (**31**)[108] and acid groups,[18,26] which all induce compatibility of the BTA with water. The application of pyridine and benzoic acid derivatives resulted in the formation of pH responsive hydrogels.[18,108] These readily accessible, reversible and responsive gels are appealing for the construction of sensors and as scaffolds for tissue engineering.

All of the examples above deal with the development of advanced materials that are far from being commercialised for the time being. A prominent success of BTA commercialisation is its application as a nucleating and clarifying agent for the bulk polymer isotactic polypropylene (*i*PP).[41,109] In the absence of additives, *i*PP crystallises at around 110 °C as an opaque material. The addition of small amounts of BTA (around 200 ppm) increases the crystallisation temperature and limits the spherulite size, which enhances the optical transparency of *i*PP. Remarkably, different structural features and solid-state order were observed in BTAs as a result of subtle structural changes in the alkyl groups and the amide connectivity.[56] Typically, when BTAs crystallize into needle-like crystals of high aspect ratios (> 50), an increase in crystallisation temperature of *i*PP (from 10 to 20 °C) was observed which was often accompanied by a significant reduction in the haze. BTA **13** was found to be the most effective in reducing the haze and improving the clarity of *i*PP.[41] Detailed X-ray structure analysis on BTA **9** (Scheme 5) revealed that the exposed side groups of one single columnar BTA aggregates form a one-dimensional lattice and thereby a regular pattern on the crystal surface of the compound.[56] The repeat distance in the *c*-direction corresponds to the spacing between the two

exposed methyl groups in *i*PP, favouring epitaxial growth of the polymer on the BTA crystal lattice. This ability is now commercialised and the most effective BTA is available as Irgaclear XT 386 from BASF. Recently, also other polymers such as poly(ethylene-*co*-propylene), poly(vinylidene fluoride) and polylactide were found to be effectively nucleated by BTAs, showing their broad application potential.[110–114] In the examples discussed above, the formation of columnar structures stabilised by threefold, intermolecular H-bonding between the disc-shaped BTA molecules is responsible for the beneficial properties observed.

5.2 BTAs in biomedical applications

Multivalent interactions allow strong and selective binding of ligand molecules to their biological targets in aqueous solutions. Because BTAs are trivalent they can serve as a convenient scaffold connecting bioactive units *via* flexible linkers.[115–119] Subsequent aggregation of trivalent BTAs then results in polyvalent molecular wires which can be used for various purposes. To this end, Brunsveld and co-workers synthesized analogues of **32** substituted with mannose units at the periphery which show fluorescence upon aggregation.[120] Strong binding to bacterial lectins was demonstrated and visualised using fluorescence microscopy. Polyvalency in the molecular wires could be tuned by mixing mannose substituted BTAs with non-functionalized BTA **32**. More recently, a family of phenylglycine and F_5-phenylglycine based BTAs was synthesised with paramagnetic Gd(III)-complexes connected to the periphery.[28,97] Depending on the molecular design, these compounds form either spherical particles with hydrodynamic radii in the nanometer range (around 5 nm) or long elongated aggregates with rod radii of 3.1 nm and lengths of the rods of 75 nm at mM concentrations. A combination of CD spectroscopy, cryo-TEM and NMR studies showed that columnar helical aggregates formed were stabilised by intermolecular H-bonding.[28,97] *In vitro* and *in vivo* experiments on the Gd(III)–DTPA based BTAs with sizes in the 6 nm range showed excellent contrast-enhanced magnetic resonance imaging (MRI) (Fig. 3D).[40] Blood circulation times allowed high-resolution angiography of the mouse brain vasculature at Gd(III) doses far below those of clinical contrast agents. The high stability and slow clearance rates, combined with their ideal size in the nanometer range, provide a powerful platform for further developments in molecular imaging.

5.3 BTAs for coordinating metal ions

Apart from their ability to form H-bonds, several BTAs comprise peripheral groups that are capable of coordinating metal ions. *N*,*N*′,*N*″-Tris(3-pyridyl)-1,3,5-tricarboxamide (**2**, Scheme 4), for example, has been explored in the formation of stable nanocages using Pd(II) and Cu(II) metal ions.[121–123] In contrast, the related *N*,*N*′,*N*″-tris(4-pyridyl)-1,3,5-tricarboxamide (**38**) formed a twofold interpenetrating network upon complexation with Cu(II) metal ions and the resulting metal–organic framework showed an extremely large solvent volume.[124] BTA **38** was also combined with Cd(II) metal ions which produced a three-dimensional porous coordination polymer.[125] The amide groups were not involved in H-bonding and occurred on the surfaces of formed channels. These highly ordered amide groups in the channels were found to play an important role in the interaction with the guest molecules, which was confirmed by thermogravimetric analysis, adsorption/desorption measurements, and X-ray crystallography. Interestingly, a Knoevenagel condensation reaction was catalyzed by the solid coordination polymer, demonstrating its selective heterogeneous base catalytic properties. The solid catalyst maintained its crystalline framework after the reaction and was easily recycled. This research is particularly interesting for the generation of new metal–organic framework (MOF) materials with functional properties such as structure absorbants and heterogeneous catalysts.[126,127]

6. Conclusions

An exponential increase in the synthesis and application of various BTA molecules and derivatives has been observed during the past decade. Owing to their simple structure and high synthetic accessibility in combination with a detailed understanding of their supramolecular self-assembly behaviour, this versatile, supramolecular building block is frequently utilized in various applications ranging from nanotechnology to polymer processing and biomedical applications. While the opportunities in the former cases are connected to the self-assembly of BTAs into one-dimensional, nanometer-sized rod like structures stabilised by threefold H-bonding, their multivalent nature drives applications in the biomedical field and in the synthesis of MOFs. The adaptable nature of this multipurpose building block in combination with the first commercial applications promises a bright future for BTA-based molecules

Acknowledgements

The authors would like to thank the Dutch National Research School Combination Catalysis Controlled by Chemical Design (NRSC-C) for financial support, Prof. Dr P. Smith (ETH Zürich) for helpful discussions and Prof. Dr E.W. Meijer (Eindhoven University of Technology) and Dr J. A. J. M. Vekemans (Eindhoven University of Technology) for continuing support. The ICMS animation studio (Eindhoven University of Technology) is acknowledged for providing artwork.

Notes and references

1 J. M. Lehn, *Angew. Chem., Int. Ed.*, 1990, **29**, 1304–1319.
2 T. Aida, E. W. Meijer and S. I. Stupp, *Science*, 2012, **335**, 813–817.
3 P. Y. W. Dankers and E. W Meijer, *Bull. Chem. Soc. Jpn.*, 2007, **80**, 2047–2073.
4 P. Y. W. Dankers, M. C. Harmsen, L. A. Brouwer, M. J. A. van Luyn and E. W. Meijer, *Nat. Mater.*, 2005, **4**, 568–574.
5 P. Y. W. Dankers, T. M. Hermans, T. W. Baughman, Y. Kamikawa, R. E. Kieltyka, M. M. C. Bastings, H. M. Janssen, N. A. J. M. Sommerdijk, A. Larsen, M. J. A. van Luyn, A. W. Bosman, E. R. Popa, G. Fytas and E. W. Meijer, *Adv. Mater.*, 2012, **24**, 2703–2709.
6 T. Curtius, *J. Prakt. Chem.*, 1915, **91**, 39–100.
7 Rohm & Haas Co, *US*, 2774750, 1956.
8 W. Ried and F. J. Koenigstein, *Chem. Ber.*, 1959, **92**, 2532–2542.
9 Bayer, *DE*, 2417763, 1975.
10 J. Roosma, T. Mes, P. Leclere, A. R. A. Palmans and E. W. Meijer, *J. Am. Chem. Soc.*, 2008, **130**, 1120–1121.

11 J. E. Gill, R. MacGillivray and J. Munro, *J. Chem. Soc.*, 1949, 1753–1754.
12 H. Stetter, D. Theise and G. J. Steffens, *Chem. Ber.*, 1970, **103**, 200–204.
13 I. Arai, Y. Sei and I. Muramatsu, *J. Org. Chem.*, 1981, **46**, 4597–4599.
14 J. J. van Gorp, J. A. J. M. Vekemans and E. W. Meijer, *Mol. Cryst. Liq. Cryst.*, 2003, **397**, 491–505.
15 Y. Matsunaga, N. Miyajima, Y. Nakayasu, S. Sakai and M. Yonenaga, *Bull. Chem. Soc. Jpn.*, 1988, **61**, 207–210.
16 P. J. M. Stals, J. Everts, R. de Bruijn, I. A. W. Filot, M. M. J. Smulders, R. Martín-Rapún, E. A. Pidko, T. F. A. de Greef, A. R. A. Palmans and E. W. Meijer, *Chem.–Eur. J.*, 2010, **16**, 810–821.
17 J. J. van Gorp, J. A. J. M. Vekemans and E. W. Meijer, *J. Am. Chem. Soc.*, 2002, **124**, 14759–14769.
18 A. Bernet, R. Q. Albuquerque, M. Behr, S. T. Hoffmann and H.-W. Schmidt, *Soft Matter*, 2012, **8**, 66–69.
19 J. Y. Chang, J. H. Baik, C. B. Lee and M. J. Han, *J. Am. Chem. Soc.*, 1997, **119**, 3197–3198.
20 A. R. A. Palmans, J. A. J. M. Vekemans, E. W. Meijer, H. Kooijmans and A. L. Spek, *Chem. Commun.*, 1997, 2247–2248.
21 A. R. A. Palmans, J. A. J. M. Vekemans, H. Fischer, R. A. Hikmet and E. W. Meijer, *Chem.–Eur. J.*, 1997, **3**, 300–309.
22 L. Brunsveld, H. Zhang, M. Glasbeek, J. A. J. M. Vekemans and E. W. Meijer, *J. Am. Chem. Soc.*, 2000, **122**, 6175–6182.
23 R. van Hameren, P. Schön, A. M. van Buul, J. Hoogboom, S. V. Lazarenko, J. W. Gerritsen, H. Engelkamp, P. M. Christianen, H. A. Heus, J. C. Maan, T. Rasing, S. Speller, A. E. Rowan, J. A. A. W. Elemans and R. J. M. Nolte, *Science*, 2006, **314**, 1433–1436.
24 I. Paraschiv, M. Giesbers, B. van Lagen, F. C. Grozema, R. D. Abellon, L. D. A. Siebbeles, A. T. M. Marcelis, H. Zuilhof and E. J. R. Sudhölter, *Chem. Mater.*, 2006, **18**, 968–974.
25 J. van Herrikhuyzen, P. Jonkheijm, A. P. H. J. Schenning and E. W. Meijer, *Org. Biomol. Chem.*, 2006, **4**, 1539–1545.
26 B. Gong, C. Zheng and Y. Yan, *J. Chem. Crystallogr.*, 1999, **29**, 649–652.
27 P. P. Bose, M. G. B. Drew, A. K. Das and A. Banerjee, *Chem. Commun.*, 2006, 3196–3198.
28 P. Besenius, G. Portale, P. H. H. Bomans, H. M. Janssen, A. R. A. Palmans and E. W. Meijer, *Proc. Natl. Acad. Sci. U. S. A.*, 2010, **107**, 17888–17893.
29 M. Gelinsky, R. Vogler and H. Vahrenkamp, *Inorg. Chem.*, 2002, **41**, 2560–2564.
30 M. de Loos, J. H. van Esch, R. M. Kellogg and B. L. Feringa, *Tetrahedron*, 2007, **63**, 7285–7301.
31 M. A. J. Veld, D. Haveman, A. R. A. Palmans and E. W. Meijer, *Soft Matter*, 2011, **7**, 524–531.
32 K. P. v. d. Hout, R. Martín-Rapún, J. A. J. M. Vekemans and E. W. Meijer, *Chem.–Eur. J.*, 2007, **13**, 8111–8123.
33 K. Matsuura, K. Murasato and N. Kimisuka, *J. Am. Chem. Soc.*, 2005, **127**, 10148–10149.
34 M. Akiyama, A. Katoh and T. Ogawa, *J. Chem. Soc., Perkin Trans. 2*, 1989, 1213–1219.
35 P. J. M. Stals, J. F. Haveman, R. Martín-Rapún, C. F. C. Fitié, A. R. A. Palmans and E. W. Meijer, *J. Mater. Chem.*, 2009, **19**, 124–130.
36 S. Lee, J.-S. Lee, C. H. Lee, Y.-S. Jung and J.-M. Kim, *Langmuir*, 2011, **27**, 1560–1564.
37 T. Shikata, D. Ogata and K. Hanabusa, *J. Phys. Chem. B*, 2004, **108**, 508–514.
38 N. Shi, H. Dong, G. Yin, Z. Xu and S. Li, *Adv. Funct. Mater.*, 2007, **17**, 1837–1843.
39 C. F. C. Fitié, I. Tomatsu, D. Byelov, W. H. de Jeu and R. P. Sijbesma, *Chem. Mater.*, 2008, **20**, 2394–2404.
40 P. Besenius, J. L. M. Heynens, R. Straathof, M. M. L. Nieuwenhuizen, P. H. H. Bomans, E. Terreno, S. Aime, G. J. Strijkers, K. Nicolay and E. W. Meijer, *Contrast Media Mol. Imaging*, 2012, **7**, 356–361.
41 M. Blomenhofer, S. Ganzleben, D. Hanft, H.-W. Schmidt, M. Kristiansen, P. Smith, K. Stoll, D. Maeder and K. Hoffmann, *Macromolecules*, 2005, **38**, 3688–3695.
42 K. E. Broaders, S. J. Pastine, S. Grandhe and J. M. J. Fréchet, *Chem. Commun.*, 2011, **47**, 665–667.
43 W. Kiggen, F. Vogtle, S. Franken and H. Puff, *Tetrahedron*, 1986, **42**, 1859–1872.
44 T. Fujita and J. M. Lehn, *Tetrahedron Lett.*, 1988, **29**, 1709–1712.
45 S. S. Yoon and W. C. Still, *Tetrahedron*, 1994, **35**, 8557–8560.
46 W.-D. Jang and T. Aida, *Macromolecules*, 2004, **37**, 7325–7330.
47 G. R. Newkome, X. Lin and J. K. Young, *Synlett*, 1992, 53–54.
48 P. R. Ashton, S. E. Boyd, C. L. Brown, N. Jayaraman, S. A. Nepogodiev and J. F. Stoddart, *Chem.–Eur. J.*, 1996, **2**, 1115–1127.
49 T. Zhou, H. Neubert, D. Y. Liu, Y. M. Ma, X. L. Kong, W. Luo, M. Sykes and R. C. Hider, *J. Med. Chem.*, 2006, **49**, 4171–4182.
50 Y. M. Chabre, D. Giguère, B. Blanchard, J. Rodrigue, S. Rocheleau, M. Neault, S. Rauthu, A. Papadopoulos, A. A. Arnold, A. Imberty and R. Roy, *Chem.–Eur. J.*, 2011, **17**, 6545–6562.
51 P. Rajakumar and R. Anandhan, *Eur. J. Med. Chem.*, 2012, **46**, 4687–4695.
52 R. Gutiérrez-Abad, O. Illa and R. M. Ortuño, *Org. Lett.*, 2010, **12**, 3148–3151.
53 M. Peterca, M. R. Imam, C.-H. Ahn, V. S. K. Balagurusamy, D. A. Wilson, B. M. Rosen and V. Percec, *J. Am. Chem. Soc.*, 2011, **133**, 2311–2328.
54 T. Mes, R. van der Weegen, A. R. A. Palmans and E. W. Meijer, *Angew. Chem., Int. Ed.*, 2011, **123**, 5191–5195.
55 T. Terashima, T. Mes, T. F. A. de Greef, M. A. J. Gillissen, P. Besenius, A. R. A. Palmans and E. W. Meijer, *J. Am. Chem. Soc.*, 2011, **133**, 4742–4745.
56 M. Kristiansen, P. Smith, H. Chanzy, C. Baerlocher, V. Gramlich, L. McCusker, T. Weber, P. Pattison, M. Blomenhofer and H.-W. Schmidt, *Cryst. Growth Des.*, 2009, **9**, 2556–2558.
57 P. J. M. Stals, M. M. J. Smulders, R. Martín-Rapún, A. R. A. Palmans and E. W. Meijer, *Chem.–Eur. J.*, 2009, **15**, 2071–2080.
58 S. Y. Ryu, S. Kim, J. Seo, Y.-W. Kim, O.-H. Woon, D.-J. Jang and S. Y. Park, *Chem. Commun.*, 2004, 70–71.
59 L. Brunsveld, A. P. H. J. Schenning, M. A. C. Broeren, H. M. Janssen, J. A. J. M. Vekemans and E. W. Meijer, *Chem. Lett.*, 2000, 292–293.
60 K. Hanabusa, C. Koto, M. Kimura, H. Shirai and A. Kakehi, *Chem. Lett.*, 1997, 429–430.
61 L. Rajput and K. Biradha, *J. Mol. Struct.*, 2008, **876**, 339–343.
62 M. P. Lightfoot, F. S. Mair, R. G. Pritchard and J. E. Warren, *Chem. Commun.*, 1999, 1945–1946.
63 B. Konig, O. Moller, P. Bubenitschek and P. G. Jones, *J. Org. Chem.*, 1995, **60**, 4291–4293.
64 C. A. Jimenez, J. B. Belmar, L. Ortiz, P. Hidalgo, O. Fabelo, J. Pasan and C. Ruiz-Perez, *Cryst. Growth Des.*, 2009, **9–12**, 4987–4989.
65 L. Rajput, C. V. Chernyshev and K. Biradha, *Chem. Commun.*, 2010, **46**, 6530–6532.
66 R. Kannapan, D. M. Tooke, A. L. Spek and J. Reedijk, *J. Mol. Struct.*, 2005, **751**, 55–59.
67 G. Srinivasulu, B. Sridhar, K. R. Kumar, B. Sreedhar, V. Ramesh, R. Srinivas and A. C. Kunwar, *J. Mol. Struct.*, 2011, **1006**, 180–184.
68 D. Ranganathan, S. Kurur, R. Gilardi and I. L. Karle, *Biopolymers*, 2000, **54**, 289–295.
69 M. Schmidt, J. J. Wittmann, R. Kress, D. Schneider, S. Steuernagel, H.-W. Schmidt and J. Senker, *Cryst. Growth Des.*, 2012, **12**, 2543–2551.
70 D. L. Caulder, C. Brückner, R. E. Powers, S. König, T. N. Parac, J. A. Leary and K. N. Raymond, *J. Am. Chem. Soc.*, 2001, **123**, 8923–8938.
71 S. Cantekin, H. M. M. ten Eikelder, A. J. Markvoort, M. A. J. Veld, P. A. Korevaar, M. M. Green, A. R. A. Palmans and E. W. Meijer, *Angew. Chem., Int. Ed.*, 2012, **51**, 6426–6431.
72 T. F. A. de Greef, M. M. L. Nieuwenhuizen, P. J. M. Stals, C. F. C. Fitié, A. R. A. Palmans, R. P. Sijbesma and E. W. Meijer, *Chem. Commun.*, 2008, 4306–4308.
73 M. Wegner, D. Dudenko, D. Sebastiani, A. R. A. Palmans, T. F. A. de Greef, R. Graf and H. W. Spiess, *Chem. Sci.*, 2011, **2**, 2040–2049.
74 T. F. A. de Greef, M. M. J. Smulders, M. Wolffs, A. P. H. J. Schenning, R. P. Sijbesma and E. W. Meijer, *Chem. Rev.*, 2009, **109**, 5687–5754.
75 M. M. J. Smulders, T. Buffeteau, D. Cavagnat, M. Wolffs, A. P. H. J. Schenning and E. W. Meijer, *Chirality*, 2008, **20**, 1016–1022.

76 S. Cantekin, D. W. R. Balkenende, M. M. J. Smulders, A. R. A. Palmans and E. W. Meijer, *Nat. Chem.*, 2011, **3**, 42–46.
77 M. M. J. Smulders, A. P. H. J. Schenning and E. W. Meijer, *J. Am. Chem. Soc.*, 2008, **130**, 606–611.
78 A. J. Markvoort, H. M. M. ten Eikelder, P. A. J. Hilbers, T. F. A. de Greef and E. W. Meijer, *Nat. Commun.*, 2011, **2**, 509–517.
79 I. A. W. Filot, A. R. A. Palmans, P. A. J. Hilbers, R. A. van Santen, E. A. Pidko and T. F. A. de Greef, *J. Phys. Chem. B*, 2010, **114**, 13667–13674.
80 C. Kulkarni, S. K. Reddy, S. J. George and S. Balasubramanian, *Chem. Phys. Lett.*, 2011, **515**, 226–230.
81 A. Sakamoto, D. Ogata, T. Shikata, O. Urakawa and K. Hanabusa, *Polymer*, 2006, **47**, 956–960.
82 Y. Nakano, T. Hirose, P. J. M. Stals, E. W. Meijer and A. R. A. Palmans, *Chem. Sci.*, 2012, **3**, 148–155.
83 C. A. Hunter, *Angew. Chem., Int. Ed.*, 2004, **43**, 5310–5324.
84 M. L. Bushey, A. Hwang, P. W. Stephens and C. Nuckolls, *Angew. Chem., Int. Ed.*, 2002, **41**, 2828–2831.
85 M. L. Bushey, A. Hwang, P. W. Stephens and C. Nuckolls, *J. Am. Chem. Soc.*, 2001, **123**, 8157–8158.
86 T.-Q. Nguyen, R. Martel, P. Avouris, M. L. Bushey, L. Brus and C. Nuckolls, *J. Am. Chem. Soc.*, 2004, **126**, 5234–5242.
87 R. van Hameren, J. A. A. W. Elemans, D. Wyrostek, M. Tasior, D. T. Gryko, A. E. Rowan and R. J. M. Nolte, *J. Mater. Chem.*, 2009, **19**, 66–69.
88 R. van Hameren, A. M. van Buul, M. A. Castriciano, V. Villari, N. Micali, P. Schön, S. Speller, L. Monsù Scolaro, A. E. Rowan, J. A. A. W. Elemans and R. J. M. Nolte, *Nano Lett.*, 2008, **8**, 253–259.
89 A. R. A. Palmans, J. A. J. M. Vekemans, E. E. Havinga and E. W. Meijer, *Angew. Chem., Int. Ed. Engl.*, 1997, **36**, 2648–2651.
90 J. Van Gestel, A. R. A. Palmans, B. Titulaer, J. A. J. M. Vekemans, E. E. Havinga and E. W. Meijer, *J. Am. Chem. Soc.*, 2005, **127**, 5490–5494.
91 T. Metzroth, A. Hoffman, R. Martín-Rapún, M. M. J. Smulders, K. Pieterse, A. R. A. Palmans, J. A. J. M. Vekemans, E. W. Meijer, H. W. Spiess and J. Gauss, *Chem. Sci.*, 2011, **2**, 69–76.
92 I. Danila, F. Riobe, F. Piron, J. Puigmarti-Luis, J. D. Wallis, M. Linares, H. Agren, D. Beljonne, D. B. Amabilino and N. Avarvari, *J. Am. Chem. Soc.*, 2011, **133**, 8344–8353.
93 J. M. Zayed, N. Nouvel, U. Rauwald and O. A. Scherman, *Chem. Soc. Rev.*, 2010, **39**, 2806–2816.
94 D. A. Uhlenheuer, K. Petkau and L. Brunsveld, *Chem. Soc. Rev.*, 2010, **39**, 2817–2826.
95 B. Rybtchinski, *ACS Nano*, 2011, **5**, 6791–6818.
96 L. Brunsveld, B. Lohmeijer, J. A. J. M. Vekemans and E. W. Meijer, *Chem. Commun.*, 2000, 2305–2306.
97 P. Besenius, K. P. van den Hout, H. M. H. G. Albers, T. F. A. de Greef, L. L. C. Olijve, T. M. Hermans, B. F. M. de Waal, P. H. H. Bomans, N. A. J. M. Sommerdijk, G. Portale, A. R. A. Palmans, M. H. P. van Genderen, J. A. J. M. Vekemans and E. W. Meijer, *Chem.–Eur. J.*, 2011, **17**, 5193–5203.
98 M. M. J. Smulders, M. M. L. Nieuwenhuizen, M. Grossman, I. A. W. Filot, C. C. Lee, T. F. A. de Greef, A. P. H. J. Schenning, A. R. A. Palmans and E. W. Meijer, *Macromolecules*, 2011, **44**, 6581–6587.
99 W. Zhang, D. Horoszewski, J. Decatur and C. Nuckolls, *J. Am. Chem. Soc.*, 2003, **125**, 4870–4873.
100 Z. Chen, N. D. Urban, Y. Gao, W. Zhang, J. Deng, J. Zhu, X. C. Zeng and B. Gong, *Org. Lett.*, 2011, **13**, 4008–4011.
101 Y. Matsunaga, N. Miyajima, Y. Nakayasu, S. Sakai and M. Yonenaga, *Bull. Chem. Soc. Jpn.*, 1988, **61**, 207–210.
102 C. F. C. Fitié, W. S. C. Roelofs, M. Kemerink and R. P. Sijbesma, *J. Am. Chem. Soc.*, 2010, **132**, 6892–6893.
103 A. Sugita, K. Suzuki and S. Tasaka, *Jpn. J. Appl. Phys.*, 2008, **47**, 8043–8048.
104 N. Mohmeyer, N. Behrendt, X. Zhang, P. Smith, V. Altstädt, G. M. Sessler and H.-W. Scmidt, *Polymer*, 2007, **48**, 1612–1619.
105 K. Kreger, P. Wolfer, H. Audorf, L. Kador, N. Stingelin-Stutzmann, P. Smith and H.-W. Schmidt, *J. Am. Chem. Soc.*, 2010, **132**, 509–516.
106 K. Hermans, I. Tomatsu, M. Matecki, R. P. Sijbesma, C. W. M. Bastiaansen and D. J. Broer, *Macromol. Chem. Phys.*, 2008, **209**, 2094–2099.
107 O. Steinar, H. M. Janssen, P. M. Fransen, M. A. J. Veld and A. R. A. Palmans, *EP*, 2, 254 26 A1, 2009.
108 D. K. Kumar, D. A. Jose, P. Dastidar and A. Das, *Chem. Mater.*, 2004, **16**, 2332–2335.
109 F. Abraham, S. Ganzleben, D. Hanft, P. Smith and H.-W. Schmidt, *Macromol. Chem. Phys.*, 2010, **211**, 171–181.
110 J. Wang, Q. Dou, X. Cheng and D. Li, *J. Polym. Sci., Part B: Polym. Phys.*, 2008, **46**, 1067–1078.
111 F. Abraham and H.-W. Schmidt, *Polymer*, 2010, **51**, 913–921.
112 P. Song, Z. Wei, J. Liang, G. Chen and W. Zhang, *Polym. Eng. Sci.*, 2012, **52**, 1058–1068.
113 H. Bai, W. Zhang, H. Deng, Q. Zhang and Q. Fu, *Macromolecules*, 2011, **44**, 1233–1237.
114 H. Nakajima, M. Takahashi and Y. Kimura, *Macromol. Mater. Eng.*, 2010, **295**, 460–468.
115 H. Kubas, M. Schaefer, U. Bauder-Wuest, M. Eder, D. Oltmanns, U. Haberkorn, W. Mier and M. Eisenhut, *Nucl. Med. Biol.*, 2010, **37**, 885–891.
116 P. R. Ashton, E. F. Hounsell, N. Jayaraman, T. M. Nilsen, N. Spencer, J. F. Stoddart and M. Young, *J. Org. Chem.*, 1998, **63**, 3429–3437.
117 C. Appelt, A. K. Schrey, A. Soederhael and P. Schmieder, *Bioorg. Med. Chem. Lett.*, 2007, **17**, 2334–2337.
118 P. Rajakumar and R. Anandhan, *Eur. J. Med. Chem.*, 2011, **46**, 4687–4695.
119 Y. M. Chabre, D. Giguère, B. Blanchard, J. Rodrigue, S. Rocheleau, M. Neault, S. Rauthu, A. Papadopoulos, A. A. Arnold, A. Imberty and R. Roy, *Chem.–Eur. J.*, 2011, **17**, 6545–6562.
120 M. K. Mueller and L. Brunsveld, *Angew. Chem., Int. Ed.*, 2009, **48**, 2921–2924.
121 P. S. Mukherjee, N. Das and P. J. Stang, *J. Org. Chem.*, 2004, **69**, 3526–3529.
122 D. Moon, S. Kang, J. Park, K. Lee, R. P. John, H. Won, G. H. Seong, Y. S. Kim, G. H. Kim, H. Rhee and M. S. Lah, *J. Am. Chem. Soc.*, 2006, **128**, 3530–3531.
123 J. Park, S. Hong, D. Moon, M. Park, K. Lee, S. Kang, Y. Zou, R. P. John, G. H. Kim and M. S. Lah, *Inorg. Chem.*, 2007, **46**, 10208–10213.
124 S. Hong, Y. Zhou, D. Moon and M. S. Lah, *Chem. Commun.*, 2007, 1707–1709.
125 S. Hasegawa, S. Horike, R. Matsuda, S. Furukawa, K. Mochizuki, Y. Kinoshita and S. Kitagawa, *J. Am. Chem. Soc.*, 2007, **129**, 2607–2614.
126 L. J. Murray, M. Dincâ and J. R. Long, *Chem. Soc. Rev.*, 2009, **38**, 1294–1314.
127 J. Y. Lee, O. K. Farha, J. Roberts, K. A. Scheidt, S. T. Nguyen and J. T. Hupp, *Chem. Soc. Rev.*, 2009, **38**, 1450–1459.